ELSEVIER

Journal of Chromatography A, 917 (2001) 1–22

JOURNAL OF CHROMATOGRAPHY A

www.elsevier.com/locate/chroma

Visualization of solute migration in chromatographic columns Influence of the frit porosity

B. Scott Broyles[a,b], R. Andrew Shalliker[a,b], Georges Guiochon[a,b,*]

[a]*Department of Chemistry, The University of Tennessee, Knoxville, TN, 37996-1600, USA*

[b]*Chemical and Analytical Science Division, Oak Ridge National Laboratory, Oak Ridge, TN, 37831-6120, USA*

Received 22 November 1999; received in revised form 15 March 2000; accepted 24 March 2000

Abstract

The dual-perspective, on-column detection method previously described was used to observe the effects of the inlet frit on the profiles of chromatographic bands. Visualization of bands of iodine was achieved by injecting its dilute solutions in carbon tetrachloride into a glass column packed with a C_{18}-bonded silica and eluted with carbon tetrachloride, which has the same refractive index as the packing material. The bands were photographed on-column with two standard 35-mm SLR cameras oriented at right angle. The photographs were scanned and the digitized images of the sample bands analyzed with proper software. A number of columns, as similar as possible, were fitted with different 2- and 10-μm porosity stainless steel frits. Subsequent analysis of the digitized band images revealed irregularities in the band shape resulting from frit contributions to band dispersion. The 2-μm frits produced more dramatic effects overall than the coarser frits. Local axial dispersion coefficient values, expressed as local reduced plate height, were calculated. The results demonstrate the possibly damaging effects of the frit on the band shape.

Keywords: Visualization of solute migration; Band profiles; Porosity; Axial dispersion; Frits; Iodine

1. Introduction

Precolumn dispersion during sample introduction onto the column can have adverse effects on the chromatographic performance. These effects are due to initial band broadening as the sample passes through the inlet frit and onto the packed bed. Typically, precolumn, on-column, and postcolumn effects are tallied together and observed in the detector response to the injection of the sample. Conventional chromatographic methods allow the estimation of the global effect of extracolumn sources of band broadening, e.g. by measuring the variance of the signal obtained by replacing the column with a zero-volume connector. However, it is very difficult, if not altogether impossible, to isolate the effects of peripheral fittings on band dispersion from those effects caused by other extra-column phenomena. Consequently, techniques that allow visualization of sample migration have received considerable attention of late.

Of these techniques, NMR is the most studied. The simplest of these NMR methods involves the use of gadolinium chelates [1–3]. Using this technique, continuous monitoring of a sample band as it migrates along the column can be achieved. The principles behind the technique were comprehensive-

*Corresponding author.

E-mail address: guiochon@utk.edu (G. Guiochon).

0021-9673/01/$ – see front matter
PII: S0021-9673(01)00623-9

ly discussed and are too detailed for discussion in this work [4–6]. Suffice to say that NMR imaging studies made by Bayer et al. [2] using this method showed the column bed to be extremely homogeneous, except for some regions near the column inlet. NMR images of gadolinium complexes during their elution showed a distorted sample band that entered the column, causing poor column performance. These deformations were blamed on inlet frit obstructions or on bed cracking as the result of uneven bed consolidation. Locally, however, the bed was found to be highly homogeneous and efficient. More refined NMR techniques allow the determination of the local axial and radial dispersion coefficients averaged over relatively small volumes [7]. They provide accurate numbers but still lack in spatial definition compared to optical methods.

More recently Lode et al. [8] sought to investigate peripheral effects such as header flow distribution and to find out how to design a distributor minimizing band dispersion. Numerical simulation was employed to probe the effects of the header design on the sample concentration distribution during injection. Experimentally, NMR techniques were used to visualize the fluid flow through the header and onto the column. The spatial resolution achieved was relatively low, however, because of the long acquisition times required and the perspective was limited to one angle of view.

A new technique was recently developed by Shalliker and co-workers to visualize viscous fingering [9] and solute migration [10,11] in HPLC columns. The technique employs glass columns and matched refractive indices of the stationary and mobile phases. Consequently, the bed is transparent and the visualization of colored sample bands can be observed. Photographic detection is used to capture images of the sample band during its migration. These photographic images are manipulated to form digital images, which allows the color density to be measured. Plots of the gray-scale density versus the bed length represent the sample distribution, which in turn reflects the 'on-column' profile of a migrating injection plug.

In the present work we probe the effects of frit porosity on the band profile during sample introduction, using the method of visualization just described. Two frit types, with 2- and 10-μm porosities, were studied. By utilizing a dual camera angle view of 90° and acquiring simultaneous photographs, the profile of the sample band entering through the column head can be analyzed for homogeneity across the column diameter. In addition, verification of inconsistencies in the flow stream, that would go unnoticed in a single perspective viewing system, can be made. Band asymmetry can be observed from two angles, thus giving a more complete picture of inlet fitting effects on band deformation.

2. Experimental

2.1. Chemicals

Reagent grade carbon tetrachloride was obtained from Sigma (St. Louis, MO, USA) and reagent grade methanol and HPLC grade dichloromethane from Mallinckrodt (Paris, KY, USA). Iodine (99.9%) was obtained from General Chemical Division (New York, NY, USA). All mobile phases were sparged with helium during the experiments.

2.2. Columns and packing material

All chromatographic experiments were performed on a 100×17 mm (I.D.) borosilicate (Pyrex) glass column supplied by Omni (Cambridge, UK). The column end fittings were prepared by the University of Tennessee workshop, machined from Delrin plastic. These fittings included a fixed length outlet fitting and an adjustable inlet fitting that allowed axial compression of the column. Stainless steel frits having a diameter of 15.9 mm and a thickness of 1.57 mm were obtained from Bodman (Aston, PA, USA).

The stationary phase used was YMC C_{18} silica (Kyoto-Fu 613 Japan). This material is spherical with a particle size distribution given as 15–30 μm and an average particle size of 21 μm. The column was slurry packed in a downward configuration with methanol as both the slurry and the packing solvent. Dichloromethane was used as the displacement solvent. The slurry was pushed into the column and

consolidated by a steady stream of methanol at a flow-rate of 9 ml/min. The inlet pressure did not exceed 250 p.s.i. (1 p.s.i.=6894.76 Pa) to avoid breaking the glass column.

The head fittings were assembled and inserted into the head of the column. The head fitting was then tightened to a torque of 0.2 m kg, which pressed the frit tightly against its holder and ensured a nearly zero dead volume clearance above the frit. Such a design has the drawback of maximizing the radial distribution problem but the advantage of maximizing also its reproducibility (see below). Differences in experimental results can arise only from differences in frit properties. The head fitting is allowed to set overnight before use. To improve visualization and minimize the cylindrical lens effect, the entire column assembly was placed into a viewing cell. The cell assembly was described in a previous communication [10].

2.3. Equipment

The chromatographic system consisted of two high-performance liquid chromatographic (HPLC) pumps (model 510, Waters Associates, Milford, MA, USA) controlled by a Waters automated gradient controller. The mobile phase was 100% carbon tetrachloride and the flow-rate 1.5 ml/min throughout. Sample injection was achieved through a Rheodyne injection valve (model 7010, Rheodyne, Cotati, CA, USA). All injection volumes were 20 μl and the sample injected was a solution of iodine in carbon tetrachloride (12 g/l). Sample visualization of the band profiles was achieved using two Pentax ZX-M SLR 35 mm cameras fitted, one with a Promaster 100 mm macro lens, the other with a Makinon 80–200 mm macro zoom lens. Kodak Ektachrome 200 ASA Professional slide film was used throughout. The photographic images were digitized using a Nikon CoolScan II (Nikon, Melville, New York, NY, USA) film scanner. All images were acquired at the maximum resolution of the scanner (2700 dots per inch). Adobe PHOTOSHOP 5.0 (Adobe Systems San Jose, CA, USA) was used to perform image manipulation. Further analysis was done using SIGMASCAN PRO 4.01 (Jandel Scientific, San Rafael, CA, USA) image analysis software.

2.4. Image collection and analysis

Dual angle visualization and photographic analysis were used in this study so that the homogeneity and symmetry of the chromatographic bands could be evaluated. For this purpose, the column was immersed in a viewing cell, a square-cross-section, chemical-resistant-plastic box with four vertical glass windows, one on each face. This cell was filled with dichloromethane [12]. The column was lighted through two of these windows and the cameras collected the images from the other two. The optical axes of these cameras were at right angles to each other. The film was developed by a commercial photographic shop (Thompson PhotoStudios, Knoxville, TN, USA). Following, the images were digitized and analyzed according to the procedure described in a previous publication [10]. Calculations involving the conversion of gray-scale intensity, the measurement of histograms, and the conversion of these intensity histograms to concentration distributions were detailed in previous publications [10,12].

These processes are too detailed to be discussed again in this study. Suffice to say that the conversion from gray-scale intensity to concentration involved the use of a calibration curve obtained from the intensity of a series of known concentration standards. The calibration curve so plotted resulted in a relationship between concentration and the intensity that was non-linear.

The following relationship gave the best fit, with a regression value (r^2) always larger than 0.995:

$$C = e^{a+b\sqrt{I}}$$

where C is the concentration, I the gray-scale intensity and a and b numerical coefficients. These coefficients are functions of the transverse distance between the column axis and the location observed [12].

3. Results and discussion

The inlet and outlet fittings, including their frits, that were supplied with the glass column were not satisfactory [9,10]. It was not possible to find a commercially available frit that exactly fitted the

internal diameter of the column (17 mm). It was found too difficult to machine-tool circular, homogeneous frits from sheets of stainless steel frit without causing obstruction of the pore network around the edges. No cookie-cutter tool with hard enough edges was available and it might have caused the same systematic deformations. The 2- and 10-μm pore size frits used were the only models commercially available. However, there was a slight but significant mismatch between their O.D.s (15.9 mm) and the column I.D. So, the frit had to be inserted into a head fitting made to custom.

This head fitting had a recessed face machined to hold the frit firmly in place while avoiding mobile phase leaks along the column wall, around the frit. The edge of the frit was approximately 0.5 mm from the wall of the column, with a ring of plastic from the frit holder squeezed between the frit and the column wall. The importance of avoiding leaks between the fitting and the column wall, with a significant fraction of the mobile phase stream bypassing the frit, will be illustrated later in this work. In all likelihood, such leaks caused by the frit not reaching the wall exactly influenced to a small degree the 'wall effect' observed, especially in the region close to the column inlet. However, when evaluating the frit effect, the study was conducted such that measurements were made no closer to the wall than approximately 0.8*R* from the column center, *R* being the column radius. Hence, all measurements reported were made at least 1.7 mm from the column wall. The design of the head fitting is shown in Fig. 1.

Mobile phase and sample entered the column through a 1/16-inch hole, centered on the inlet frit. No distributor was employed in this work, which is the conventional situation in analytical applications of chromatography. The addition of a flow distributor and the effects of the diameter of the frit in relation to the column I.D. were discussed previously [13]. It was shown that available distributors did not provide a significant reduction of the band broadening. The frit was unable to ensure an homogeneous radial distribution of the incoming stream, which is why the results obtained with the best frits are not entirely satisfactory. Different results obtained with different frits may be explained by differences in the frit properties.

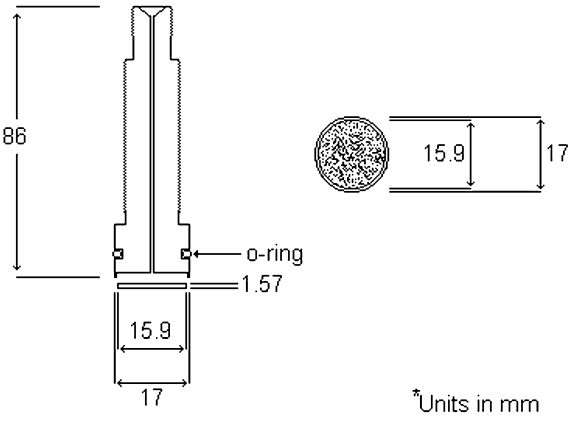

Fig. 1. Diagram of the column header containing the frit.

3.1. Sample introduction through 2-μm frits with lateral leaks

The importance of a multiaspect visualization technique is emphasized by the results obtained in the analysis of the 2-μm frits. Having a small pore size, their permeability is low. As a consequence, the liquid phase, which always takes the path of least resistance, tended to leak around the frit, along the column wall. This effect was illustrated in a particularly dramatic fashion by the results obtained with a first, incorrect design of the head fitting. Fig. 2a and b are photographs illustrating the entrance of an iodine sample moving in from this head fitting containing a 2-μm frit. From this single aspect, the profile appeared to elute from both the column center and the wall region, with a crown shape [14], but to be still reasonably uniform. However, this assumption is falsified by the second aspect, taken at a right angles. The photographs in Fig. 2c and d clearly illustrate that the sample entered the column mainly between the frit and the wall of the head piece. However, the sample stream around the frit is not homogeneous, much like the rivulets around a glass of wine (although for a different reason).

Using a technique previously described [10,12], the column was divided into vertical slices (usually 19 but, in some instances, only 11 of these slices were evaluated) parallel to the column axis and to the optical axis of the corresponding camera (see later figures, e.g. Fig. 3, for a projection of these slices on a column cross-section). The width of each

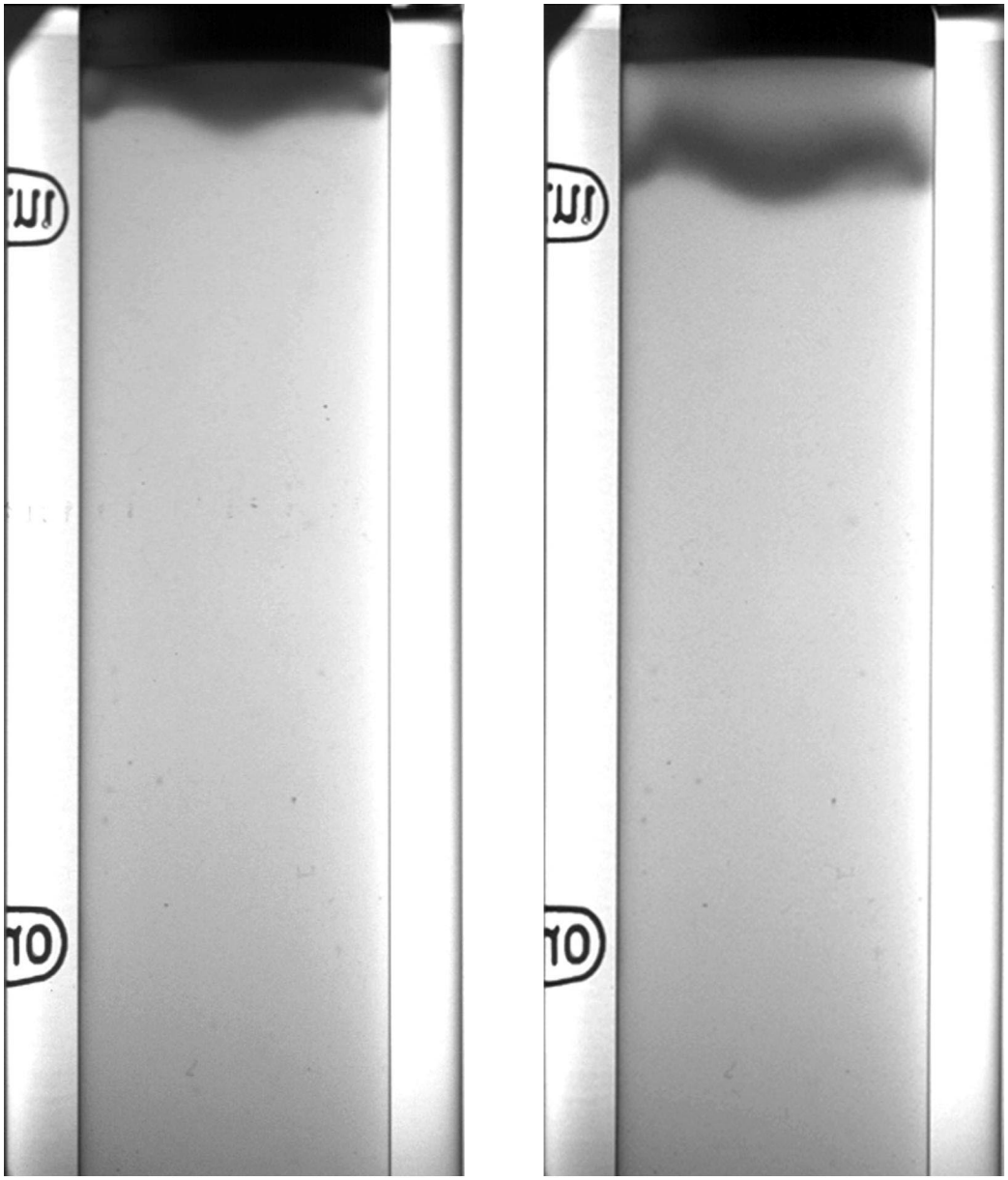

Fig. 2. Photographs of a band of iodine entering a column fitted with a 2-μm frit that leaked around its edges. (a,b) Photographed from camera 1, (c,d) photographed from camera 2, at right angles to camera 1. (a,c) Taken after 21 s, (b,d) after 45 s. Flow-rate = 1.5 ml/min.

slice was constant (0.81 mm), but not their area or their volume which are proportional to the length of the corresponding chord. The grey-scale density was measured along each section, giving histograms that reflected the radial distribution of the migration profile of the band in the direction perpendicular to the axis of view [10]. The gray-scale intensity does not reflect directly the concentration distribution of

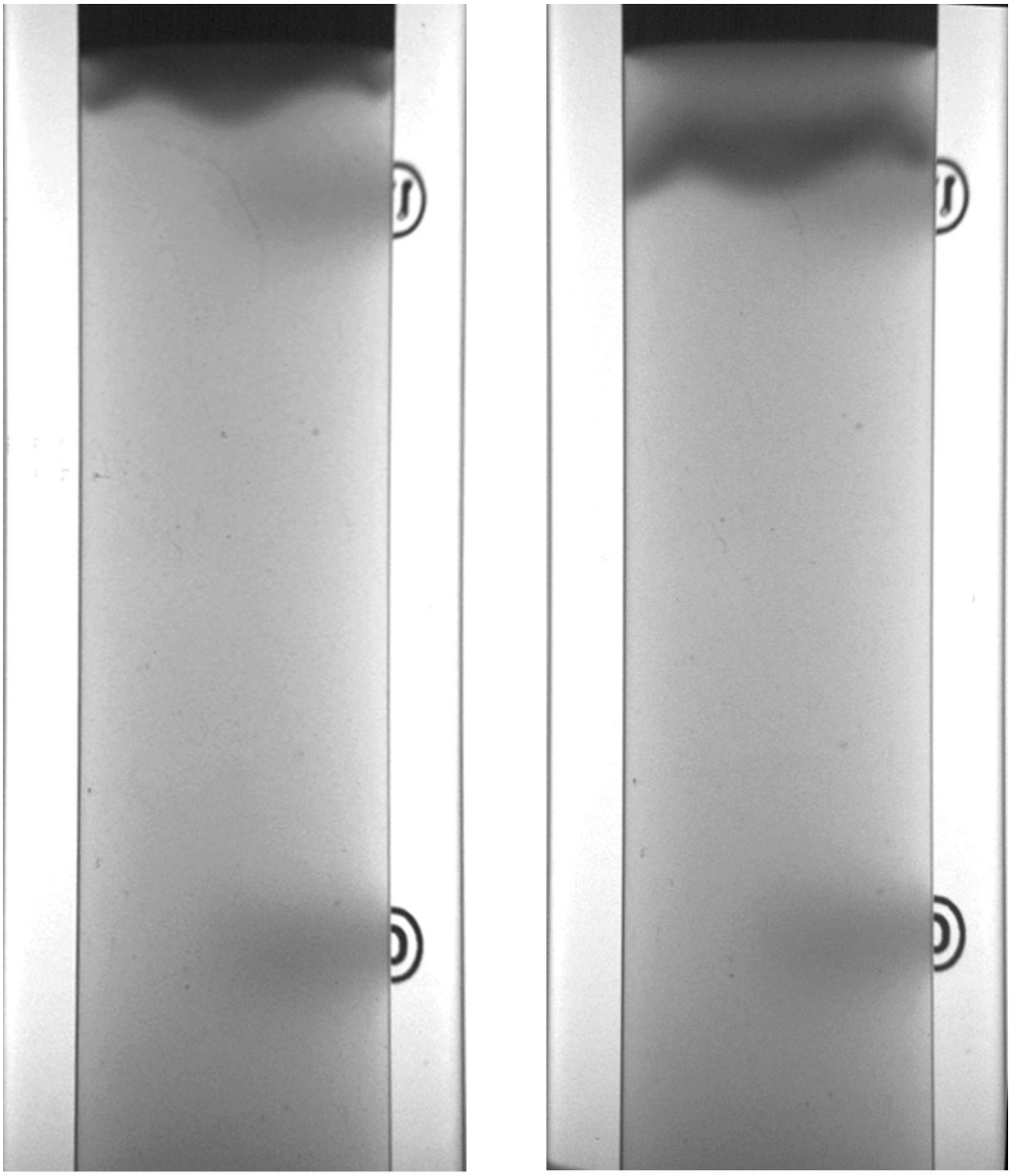

Fig. 2. (*continued*)

the sample because the column cross-section is circular, so the optical path length varies across the column diameter. In order to determine the concentration distribution, the gray-scale intensity was calibrated against the intensity obtained with a known series of standards, as described elsewhere [12]. The gray-scale intensity of the standards were determined at each of the 19 sections. A series of 19 calibration curves, each one pertaining to an identified section, were thus prepared. They allowed for

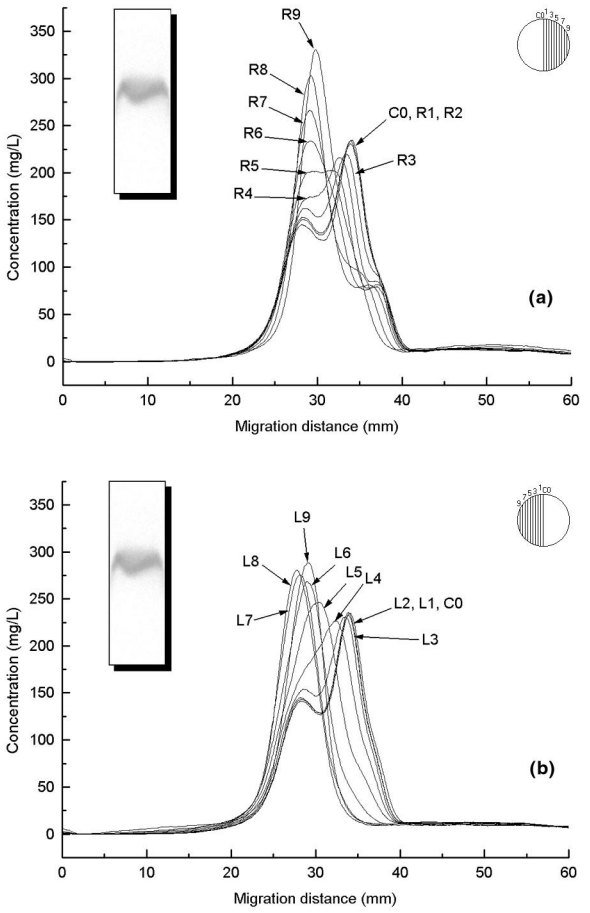

Fig. 3. Axial concentration profiles obtained by scanning the vertical bands (whose horizontal traces are shown in the right inset) of the image in the right inset, obtained with camera 1, 3 min after sample injection on column 1. The photograph was taken under the same conditions as in Fig. 2a and b. Each band is 0.81 mm wide (approximately 40 particle diameters). The image was divided into 19 sections radially across the column, as indicated in the right inset. (a) Profiles for the left hand side of the column including the center. (b) Profiles for the right hand side of the column including the center.

the determination of the concentration distribution along each of the 19 sections [12].

Fig. 3a and b illustrates these migration profiles for the sample depicted in Fig. 2. The insets of the figures show (a) the photograph from which the band profiles were measured and (b) the slice distribution. Note that the sample zone is highly distorted as a result of the leak of the mobile phase around the frit edge (compare to figures shown later in the text, e.g. Fig. 5). For the sake of clarity, Fig. 3a represents only the ten migration profiles recorded on the left hand side (LHS) of the column and the central migration profile while Fig. 3b represents the migration profiles on the right hand side (RHS) and the central migration profile. The overlay of these migration profiles verifies that the sample band moved through the frit and along the first 20 mm of the bed with a velocity which was highly variable across the column. Some of these migration profiles are poorly shaped and many form split peaks as a result of a bimodal sample distribution across the column inlet. A large part of the sample enters the column in the central region and moves fast. Another large part enters along the wall but moves more slowly (the permeability of slurry packed beds is lower close to the column wall). Finally, only a relatively small part of the sample enters the column through the intermediate region (through which it moves at an intermediate velocity).

As will be demonstrated later [13], this nonhomogeneous distribution does not result (at least at this stage, at this high degree) from the lack of a distributor. Although we know that conventional wisdom among chromatographers recognises such bimodal peak profiles and frit problems, we are not aware of any publications that have addressed this issue in any detail. Chromatographers are well aware of the fact that small pore-size frits have a low permeability. Consequently, most encased frits, unless carefully designed and manufactured, may be subjected to a similar malfunction. In addition, all frits fitted into columns should be sealed tightly to the wall or the head fitting, so as to avoid such an effect.

3.2. Sample introduction through 2-μm frits without lateral leaks

In order accurately to evaluate the performance of 2-μm frits without leaks between the frit edge and the column wall, a thin piece of PTFE tape was used to seal around the frit edges.

This process was difficult to implement. To ensure a leak proof seal, the head fitting was inspected before insertion into the column by evaluating the fluid flow through the frit. The head fitting was inverted and the flow of the fluid observed. Once

evaluated, the head fitting was inserted into the column. Two different 2-μm frits were prepared in this manner. Fig. 4a and b shows photographs illustrating the sample band eluting from the first of these 2-μm frits, at two different times. These results relate to the column labeled column 1. The symmetry of the band is verified by the photograph in Fig. 4c, which was recorded simultaneously to the second one (Fig. 4b) but at right angles. The sample entered the column in the central region prior to the wall region, resulting in a parabolic profile. This resulted in a radial variation of the migration distance of the band, as illustrated by the overlay of the axial profiles determined in the different slices and shown in Fig. 5a (LHS) and Fig. 5b (RHS).

Clearly the central region of the sample band migrated fastest. This could have been a direct result of the lack of a distributor or of a nonhomogeneous packed bed. This was not so, as will be demonstrated by results discussed later (Figs. 6–9 curves b), results which were obtained with the very same frit, this time fitted to a column of lower efficiency but yielding a similar distribution of migration distances. Also, studies with the 10-μm frits add support to the effect of the frit irrespective of the column. We attribute this effect to a radial heterogeneity of the inlet frit itself, possibly as a consequence of the frit manufacturing process. Since the inlet and outlet pressures are the same over the entire respective cross-sections of the column, radial differences of the local velocities can be explained only by a radial distribution of the column permeability. In this instance, the permeability was lower along the streamlines located in the peripheral region and consequently less sample was distributed to the wall, as can be seen in Fig. 5 and also in the plots of normalized area versus the normalized column radius shown in Fig. 6a. In Fig. 6 the area of each concentration profile for each radial section was normalized to the area of the concentration profile for the central section of the column. The plot therefore reflects the concentration distribution relative to the column axis. As a result we can clearly see that the sample distribution was slightly heterogeneous across the column, with the concentration in the RHS being nearly 20% lower than that in the LHS. The effect being nearly the same for two different columns, it must probably be traced to the injection or the distribution process of the sample. Finally, we observed with certain frits marked local fluctuations of the sample distribution superimposed upon the effects of a nonhomogeneous radial flow distribution.

The migration profiles obtained with our procedure allow the determination of the local axial dispersion coefficient and the evaluation of the column efficiency along each stream-path averaged over the migration distance considered. Using the number of theoretical plates derived from the peak width at half height of the axial concentration profiles, a plot of plate height (h) versus the normalized column radius (Fig. 7a) can be derived. This plot shows that the column is reasonably homogeneous in the central region, but that its efficiency decreases markedly toward the wall. The mean local value of h was 2.7, which also verified that the column was rather well packed, despite the low packing pressures which had to be employed in this study, using glass columns. Because of the parabolic profile of the concentration distribution at the inlet fitting (Fig. 4), the overall ‘on-column’ sample band profile obtained by summing the contributions from the individual sections weighed by their respective surface areas yielded a reduced h value of 5.2 (from peak width at half-height). Further results (not discussed here) falsified the assumption that the design of the outlet fitting would be unimportant. On the contrary, the outlet fitting also influences the peak shape to a large degree. Consequently, regular detector responses did not reflect correctly the true band profile and compared poorly to the migration profiles obtained by proper integration of the ‘on-column’ band profiles. In a previous study [12], which describes the calibration process, we compared the elution profile obtained by integration of the on-column migration profiles to that recorded from a regular on-line detector analyzing the bulk eluent at the column exit. The agreement was reasonable, but differences did exist due in most part to the outlet fitting. Consequently, we have not illustrated conventional detector generated responses in this study. In a future communication we will address in more detail this problem [13].

A second column (labeled column 2) was prepared using the same frit with which the images shown in Fig. 4 were recorded. The results were

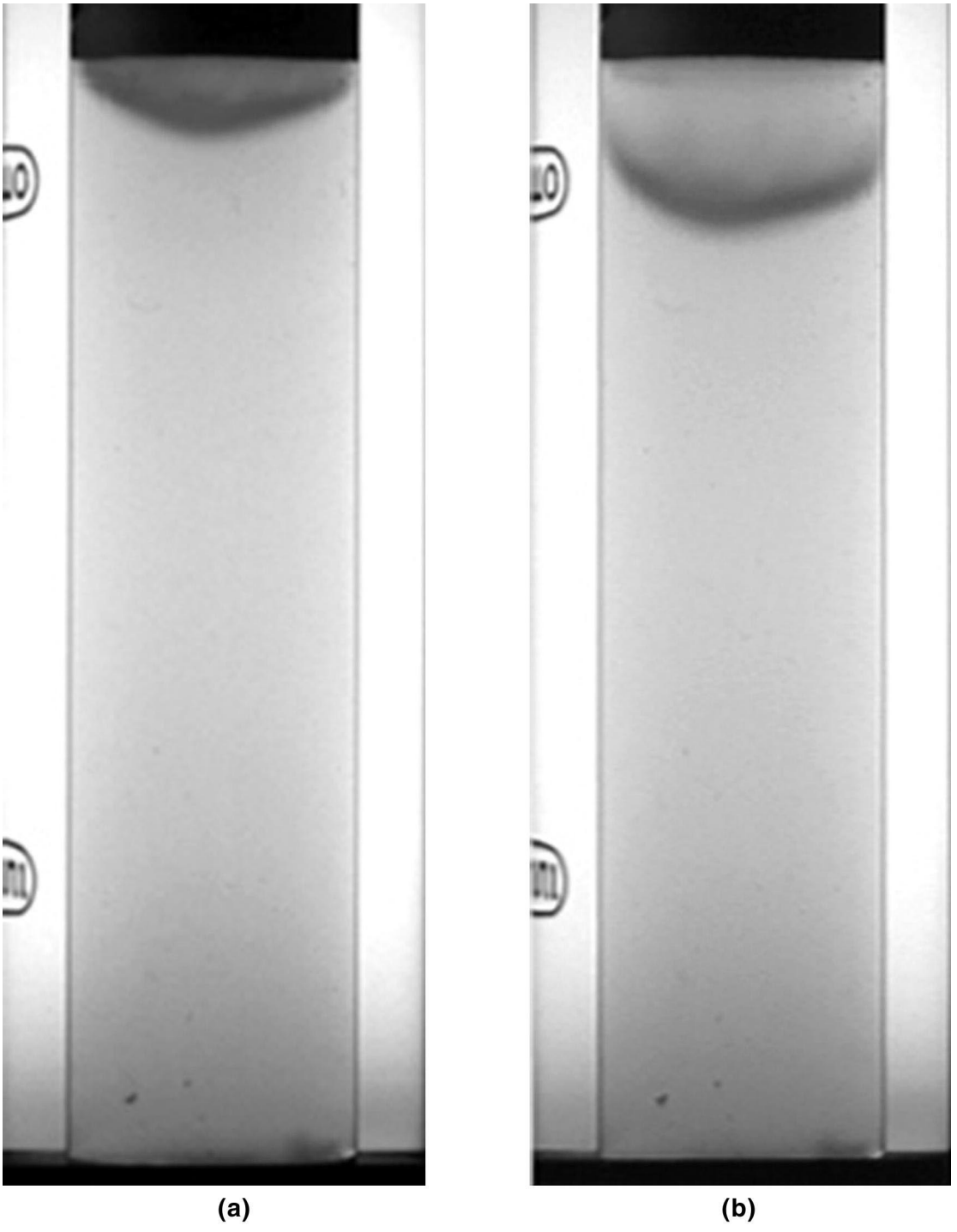

Fig. 4. Photographs of an iodine band entering a column fitted with a 2-μm frit that did not leak around the edges. (a,b) Photographed from camera 1. (c) Photographed from camera 2, at right angles to camera 1. (a) Taken after 25 s, (b,c) after 60 s. Flow-rate = 1.5 ml/min.

(c)

Fig. 4. (*continued*)

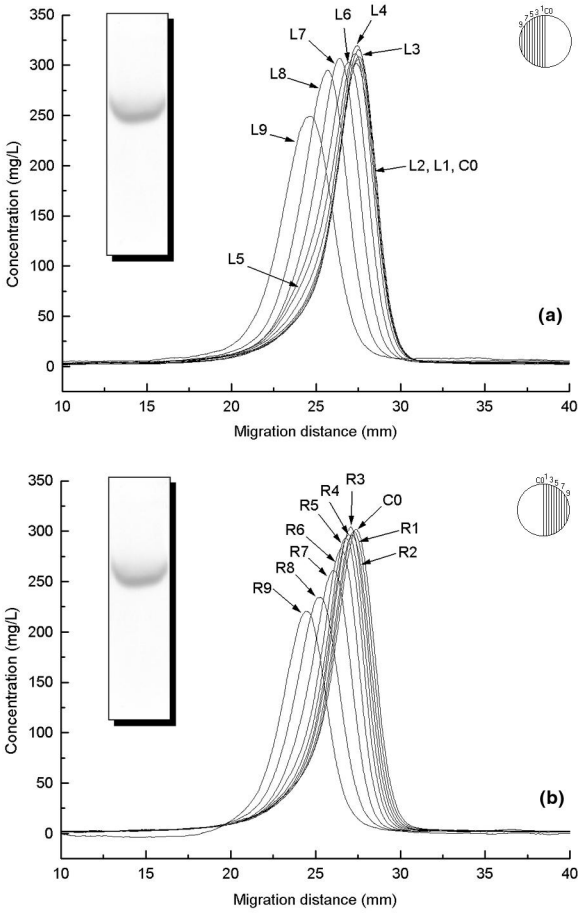

Fig. 5. Axial concentration profiles obtained by scanning the vertical bands of the image in the left inset, obtained with camera 1 3 min after sample injection on column 2, under the same conditions as in Fig. 4a and b. Each band is 0.81 mm wide (approximately 40 particle diameters). The image was divided into 19 sections radially across the column. (a) Profiles for the LHS of the column including the center. (b) Profiles for the RHS of the column including the center.

similar to those just described for column 1 for the sample concentration distribution (see Fig. 6b) but not for the column efficiency (Fig. 7). The slight differences in iodine concentration close to the wall of the two columns may be due to a change in the alignment of the frit within the head fitting and in its placement within the column. It is almost impossible to align the frit exactly the same way twice. By contrast, the efficiency of the second column is nearly a third lower than that of the first one. Plots of

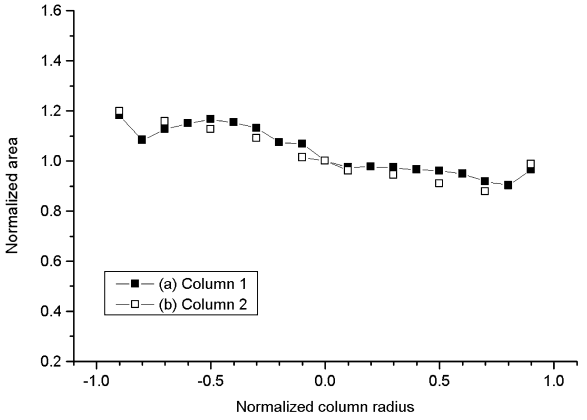

Fig. 6. Plot of the area under each concentration profile in Fig. 5, normalized to the area of the central band profile, versus the column radius. The area under the central band profile is taken as unity. (a) Column 1, head fitting containing a 2 μm frit. (b) Column 2 same head fitting as in column 1, but on a new column.

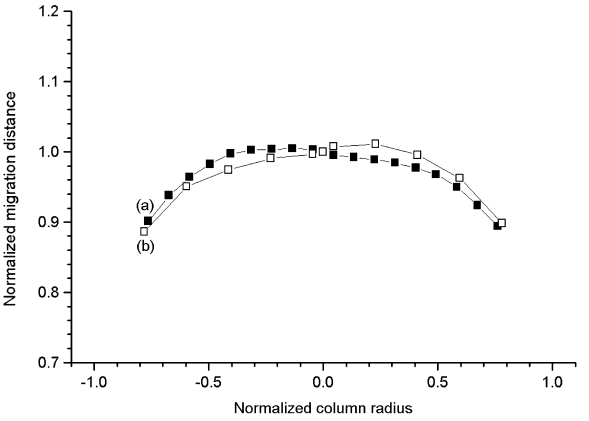

Fig. 8. Plot of the migration distance of each profile in Fig. 5, normalized to the migration distance of the central band profile, versus the column radius. (a) column 1, (b) column 2. Both columns used the same 2-μm inlet frit.

the normalized migration distance versus the normalized column radius revealed that the velocity distribution of the migration profiles were almost exactly the same, as shown in Fig. 8. This also illustrates that the fitting of the frit into the header was achieved in a reproducible manner and had no influence on the frit behavior. The velocity distribution is a function of the bed properties, and is independent of the frit. Finally, a plot of the normalized reduced plate height versus the normalized column radius shows significant differences but no clear trend. We attribute these differences to the lack of symmetry and of homogeneity of the frits.

The behavior of the second 2-μm frit was evaluated on a third column. The photographs in Fig. 10a and b shows the profile of the sample distribution at the column inlet. This profile was significantly parabolic, more so than in the photographs in Fig. 4. More importantly, however, visualization from two orthogonal angles (Fig. 10a and b represent photographs taken simultaneously) verified that the sample band entered the column slightly off center, illustrating the heterogeneity of the frit. Again, these images

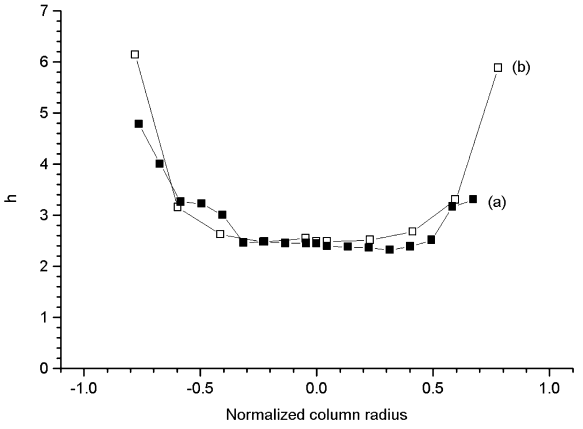

Fig. 7. Plot of the reduced plate height versus the radial location. (a) For column 1 (see the photographs in Fig. 4). (b) For column 2, fitted with the same frit as column 1.

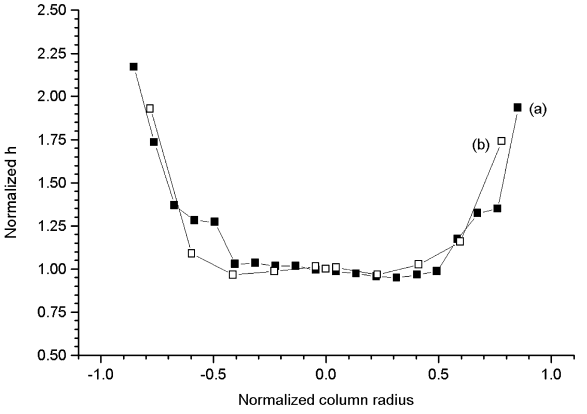

Fig. 9. Plot of the reduced plate height of each profile in Fig. 5, normalized to the reduced plate height of the central band profile, versus the column radius. (a) column 1, (b) column 2.

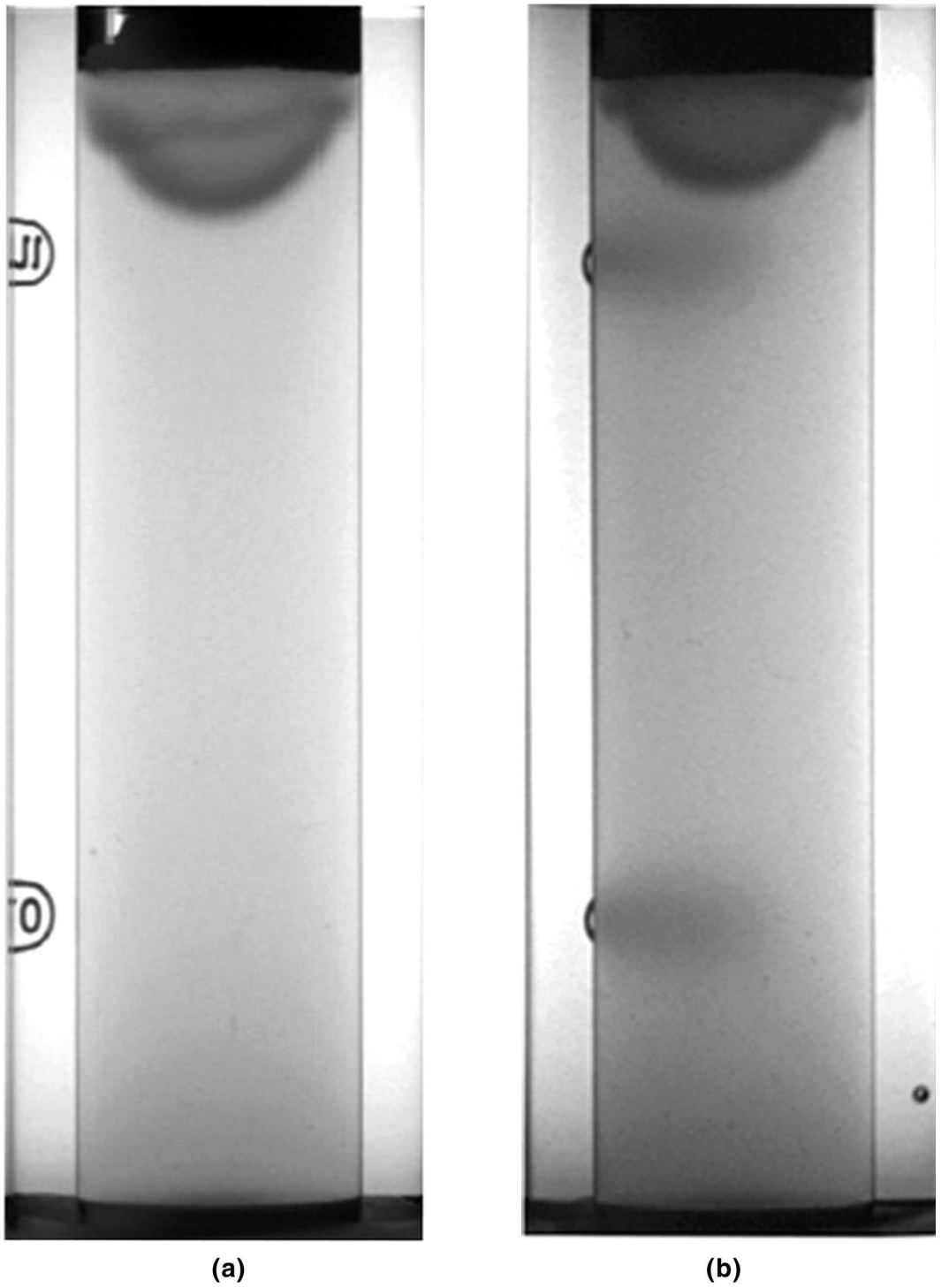

Fig. 10. Photographs of an iodine band entering a column that contained a 2-μm frit that did not leak around its edges. (a) Camera 1 and (b) camera 2; the cameras were mounted at right angles to each other; the photographs were taken after 29 s. Flow-rate = 1.5 ml/min.

show the importance of a multiaspect visualization technique (although the observer can turn around the column, it is difficult to see two images at once). As a consequence of the off-centerness of the injection, the column efficiency was found to be low and peak splitting was observed in the concentration profiles determined along the different column slices, in contrast with those reported in Fig. 5, which are typical of chromatographic bands. The multimodal nature of these profiles prevented the acquisition of any meaningful information regarding the column efficiency.

3.3. Sample introduction through 10-μm frits

Fig. 11a and b presents photographs illustrating the introduction of an iodine sample entering into the column through a 10-μm frit. The photographs in Fig. 11c and d were recorded at exactly the same time as those in Fig. 11a and b, respectively, but at right angles. Their comparison verifies the symmetry of the injection plug. In this instance, the sample band was nearly flat and plug-like. The sample concentration appeared to be uniformly distributed across the column. The migration profiles shown in Fig. 12a (LHS) and Fig. 12b (RHS) illustrate that the sample band moved through the frit and the head of the column at a velocity which is constant across the column. The small band in the rear of the profile is an artifact of unknown origin which occurs only rarely and, when it takes place, does not migrate during the course of the experiment. The surprising result is that the radial distribution of iodine concentration is the reverse of that obtained with the 2-μm frit. The sample concentration is highest in the area nearest the column wall and lowest in the central region (the widths of the peaks in Fig. 13 are nearly constant while their height increases with increasing radial distance). The local efficiency, derived from the peaks in Fig. 12 show a very homogeneous column bed (Fig. 13a).

The mean value of h derived from the width of the peaks at half-height was 3.2. This result confirms that neither the inlet fitting nor the frit itself initiated a heterogeneous distribution of the radial migration velocity of the solute, despite the slightly nonuniform concentration distribution. The overall migration profile obtained by summing up the 19 individual profiles is uniform and nearly symmetrical, as would be expected, given the overlaid profiles shown in Fig. 12. The column efficiency measured from this profile was $h = 3.3$, close to the average value of the 19 profiles. By comparison, the overall column efficiency with the 2-μm frit was much lower than the efficiency of any of the individual slices (5.2 compared to 2.7).

Several other 10-μm frits were tested to determine the degree of repeatability of the frit performance. None gave better overall performance than the first one described above (Figs. 11–13). For example, Fig. 14a and b illustrates the sample entry into the column through a second 10-μm frit. The degree of symmetry of the band is illustrated by a comparison of these figures and of Fig. 14c and d, taken at right angles to those in Fig. 14a and b, respectively. Following image analysis, on-column migration profiles taken from the sample injected in Fig. 14 resulted in the profiles shown in Fig. 15a and b (LHS and RHS). In this case, there are some significant variations of the migration distance depending on the radial location, although these variations are small compared to those observed with the 2-μm frits tested (see Figs. 3 and 5). These variations are most significant near the column wall (curves L5 and R5 in Fig. 15). The plot of h (half-height method) versus the normalized column radius (Fig. 13b) shows that the column was quite homogeneous — except near the column wall. The mean value of h was 2.8. Despite the variation of the HETP close to the wall, the overall efficiency of the migration profile taken from the sample band as a whole was equal to $h = 2.7$. These values are better than for the previous column, but the half-height method does not take into consideration the peak tailing, which was more apparent on this column.

Comparison of Figs. 11a and b and 14a and b illustrate the differences that can be observed between injection profiles into different columns, through different frits, although the end result (i.e. the apparent column efficiency) is comparable. Unfortunately, removing the head fitting to change the frit perturbs the packed bed too much and prevents from making these experiments with different frits on the very same column. Still, an informative comparison between the effects of different frits on the column characteristics is obtained by considering

Fig. 11. Photographs of an iodine band entering a column that contained a 10-μm frit. (a,b) Photographed from camera 1. (c,d) Photographed from camera 2. (a,c) Taken after 18 s, (b,d) after 30 s. Flow-rate = 1.5 ml/min.

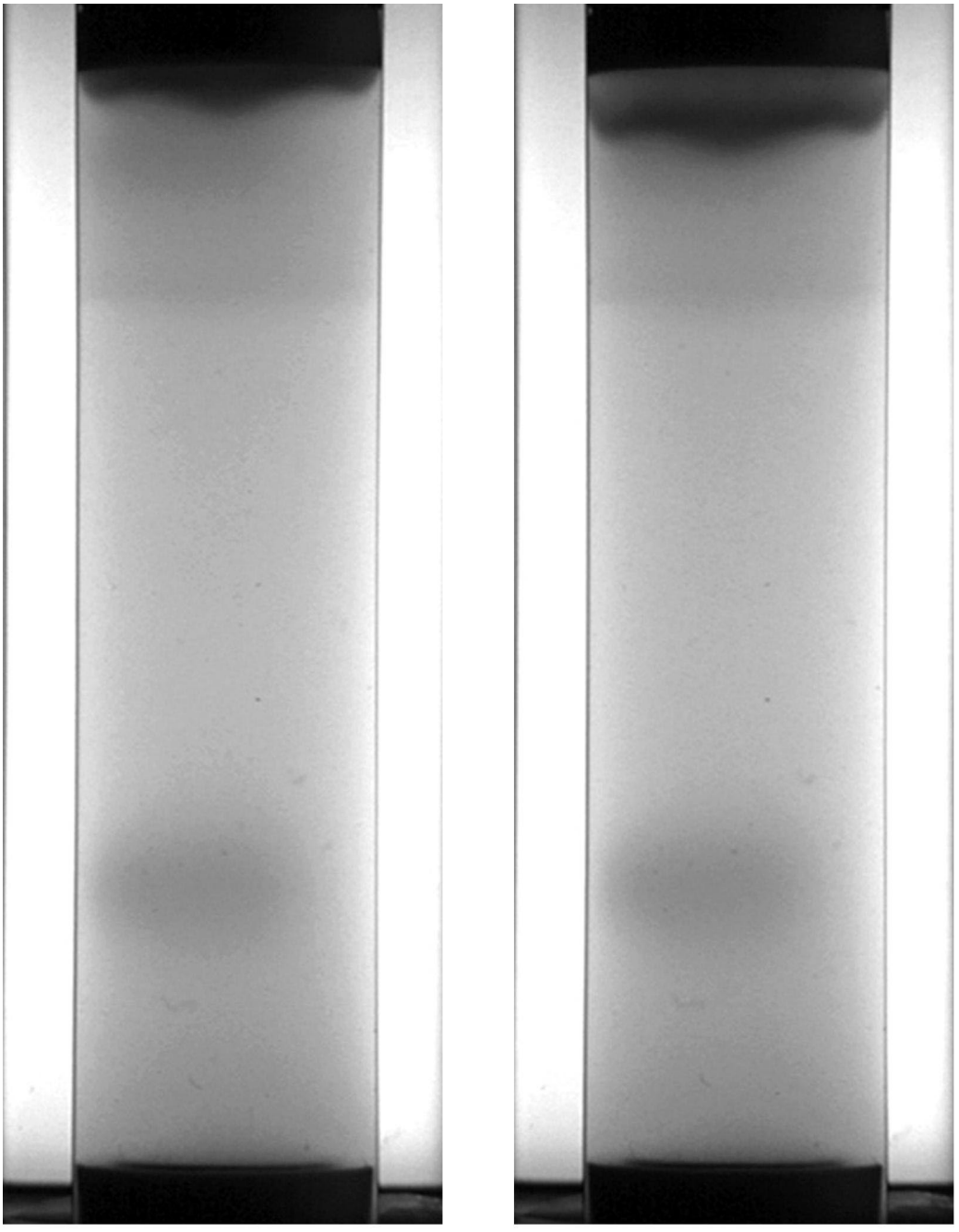

Fig. 11. (*continued*)

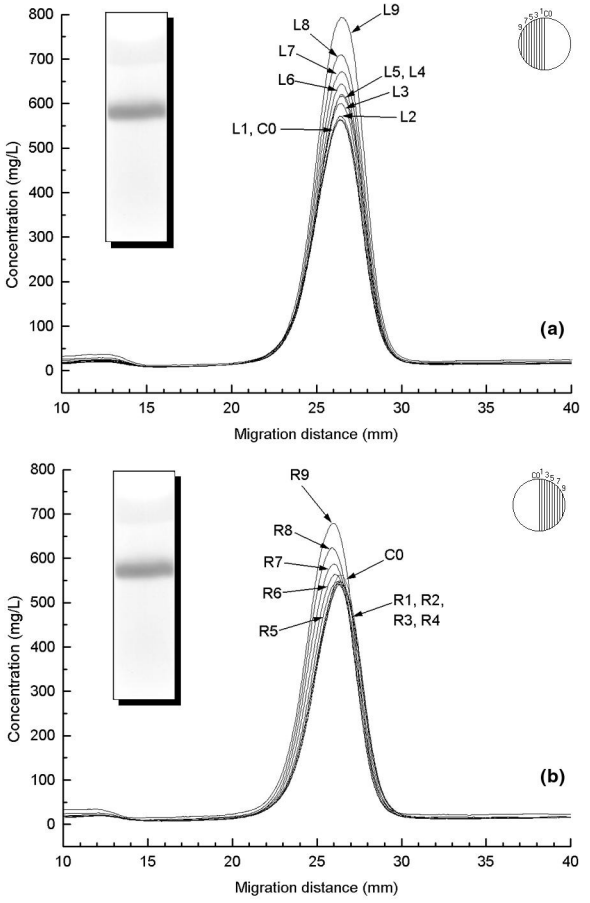

Fig. 12. Axial concentration profiles obtained by scanning the vertical bands of the image in the left inset, obtained with camera 1 three min after sample injection on the column. The photograph was taken under the same conditions as in Fig. 11a and b. (a) Profiles for the LHS of the column, including the center. (b) Profiles for the RHS of the column, including the center.

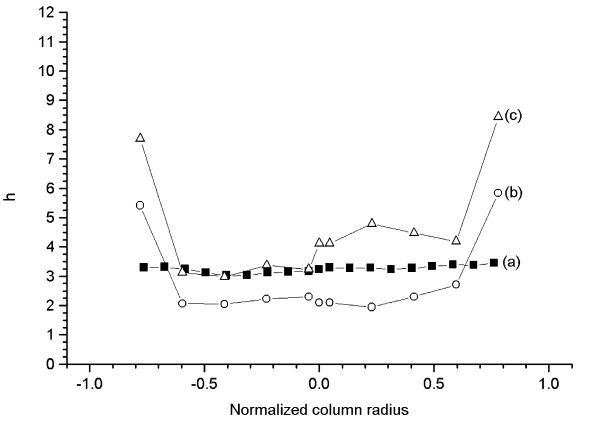

Fig. 13. Plot of the reduced plate height versus the radial location. (a) Column containing the 10-μm frit from which the photograph in the inset of Fig. 12 were obtained. (b) Column containing a second 10-μm frit, with which the photographs in Fig. 14 were obtained. (c) Column containing a third 10-μm frit, with which the photographs in Fig. 18 were obtained.

normalized parameters. Fig. 16 shows the plots of the normalized migration distance versus the normalized column radius. In this plot, the migration distance of the sample in each slice was normalized to the central migration distance. There is a clear correspondence between curves a and b and the band shapes seen in Figs. 11 and 14, respectively. The photographs of the band obtained with the third frit are shown in Fig. 18 (see below). Likewise, a direct comparison of the distributions of the iodine concentrations is illustrated in Fig. 17. Surprisingly, the sample distributions obtained with the first two frits (curves a and b) are nearly mirror images, with the second of the 10-μm frits distributing less sample to the wall region.

Not all the 10-μm frits yielded efficient performance. Fig. 18a and b illustrates the entrance profile of the sample band through the third 10-μm inlet frit. These two images were taken at right angles. They verify that the band symmetry depends on the frit used (compare with Figs. 11 and 14). The concentration profiles along the 19 slices (not shown) revealed a high degree of variation in the migration velocity across the column, as illustrated by the plot of the normalized migration distance versus the normalized column radius (Fig. 16c). Furthermore, the plot of the efficiency versus the normalized column radius (Fig. 13c) shows a wider extent of variations of the local column efficiency across the column. The RHS of the column appears to be a region of lower efficiency than the LHS. The responsibility of the frit heterogeneity is further supported by the plot of the normalized peak area versus the normalized column radius (Fig. 17c). Note that less sample was distributed on the RHS of the column, indicating that the inlet frit was highly heterogeneous. The overall efficiency of the band was poor ($h = 6.2$), due to the combination of higher local values of h and important radial variations of the migration distances (hence of the mobile phase

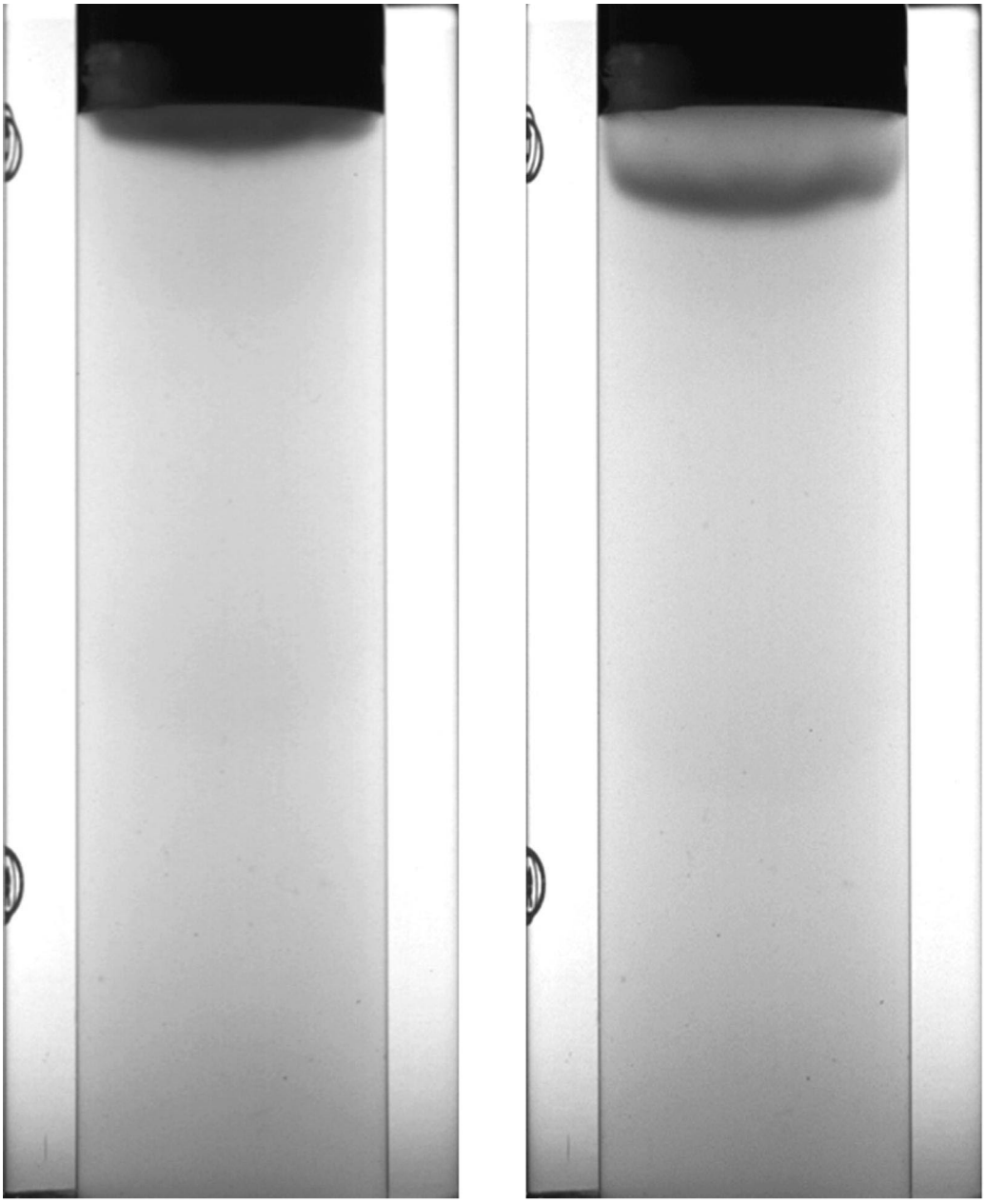

Fig. 14. Photographs of an iodine band entering the column that contained the second 10-μm frit. (a,b) Photographed from camera 1. (c,d) Photographed from camera 2. Flow-rate = 1.5 ml/min.

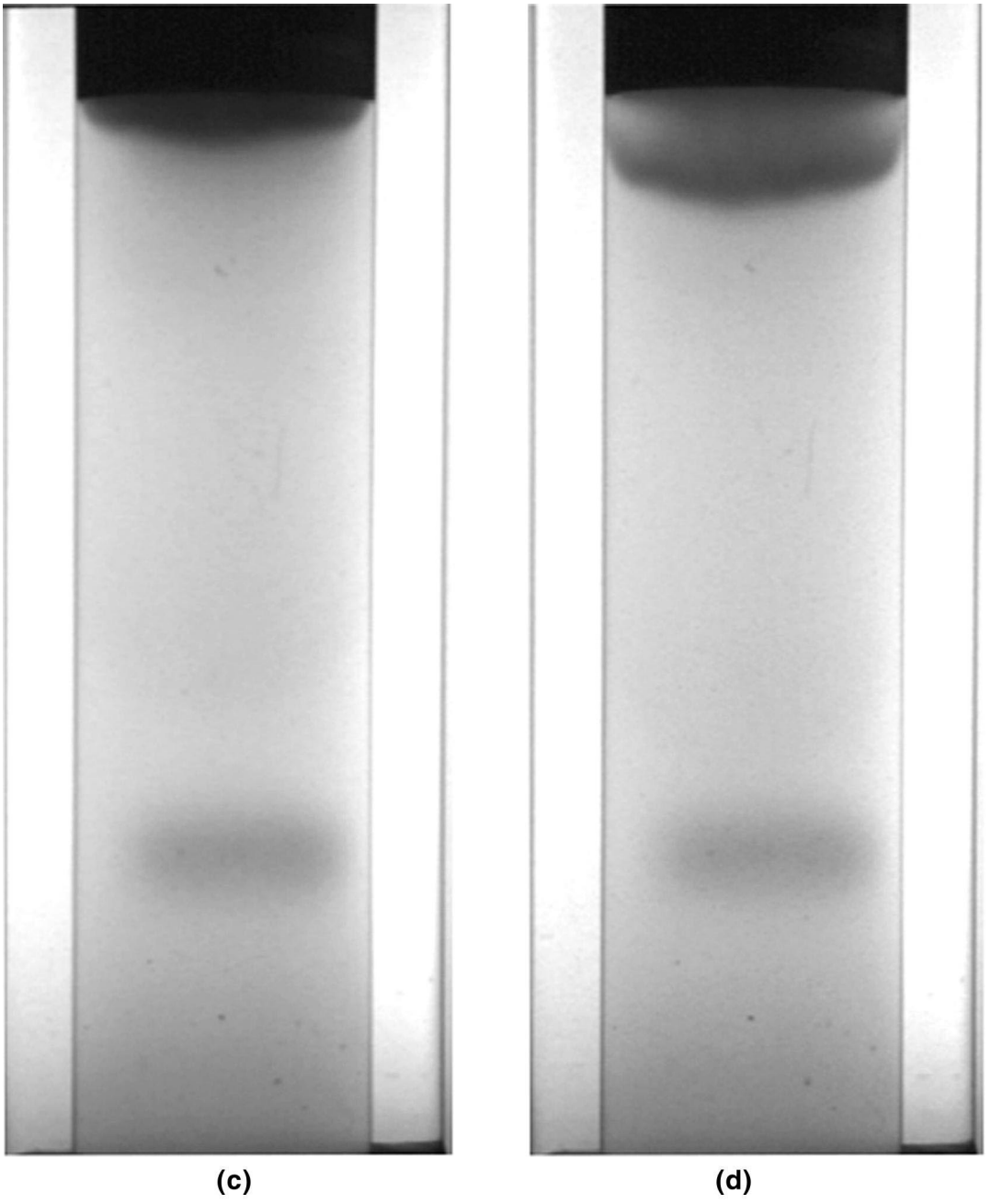

Fig. 14. (*continued*)

velocities, see Fig. 16) across the column. We attribute these variations mostly to the frit, because of the results obtained earlier (Figs. 8 and 9 regarding the 2-μm frit). Finally, note that the excellent results obtained with the first frit are probably explained by its radial heterogeneity, since it lets more sample access the wall region than the core region of the bed (Fig. 17a).

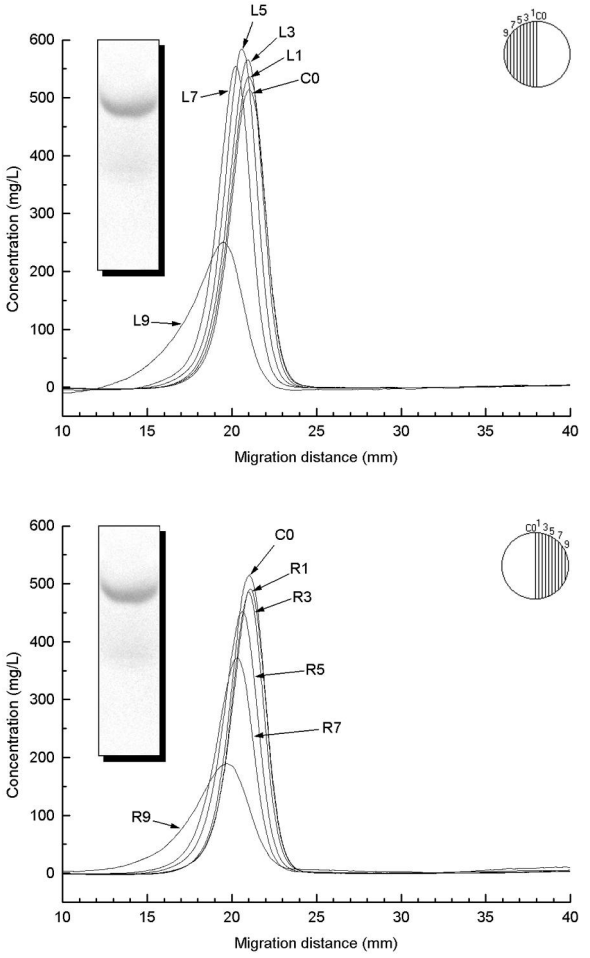

Fig. 15. Axial concentration profiles obtained by scanning the vertical bands of the image in the left inset obtained with camera 1 two min after sample injection on the column. The photograph was taken under the same conditions as Fig. 14a and b. The column was divided into 19 slices but only the data for 11 slices are shown. (a) Profiles for the LHS of the column including the center. (b) Profiles for the RHS of the column including the center.

In a study of this type it is difficult not to compare the results obtained with the two types of frits. This comparison relies on the assumption that the other factors influencing the terms of the comparison remain constant. However, a new column had to be made each time that the frit was changed. It must be assumed that the performance of all the columns packed was constant, or that their small variations do not effect the sample introduction. The data in Figs.

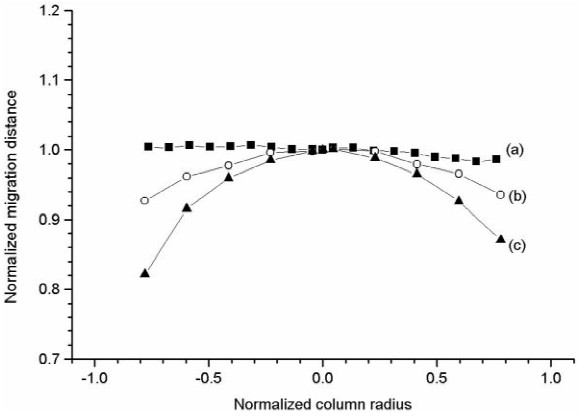

Fig. 16. Plot of the migration distance of the axial concentration profiles normalized to the migration distance of the central band profile, versus the column radius. (a) Column containing the first 10-μm frit with which the photographs in Fig. 11 were taken. (b) Column containing the second 10-μm frit with which the photographs in Fig. 14 were taken. (c) Column containing the third 10-μm frit with which the photographs in Fig. 18 were taken.

7–9, 13 and 16 support this assumption, which validates the comparisons between the performance of the different frits. Overall, the 10-μm frits proved to lead to markedly higher efficiency peaks through less intense extra-column band broadening, less tailing of the elution band and a more homogeneous radial distribution of the sample. If the column performance was reproducible, the radial distribution

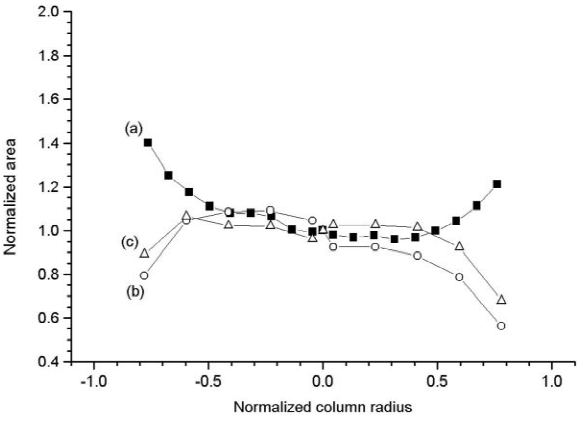

Fig. 17. Plot of the area under the axial concentration profiles, normalized to the area of the central band profile, versus the column radius. (a) Column containing the first 10-μm frit (see Fig. 11). (b) Column containing the second 10-μm frit (see Fig. 14). (c) Column containing the third 10-μm frit (Fig. 18).

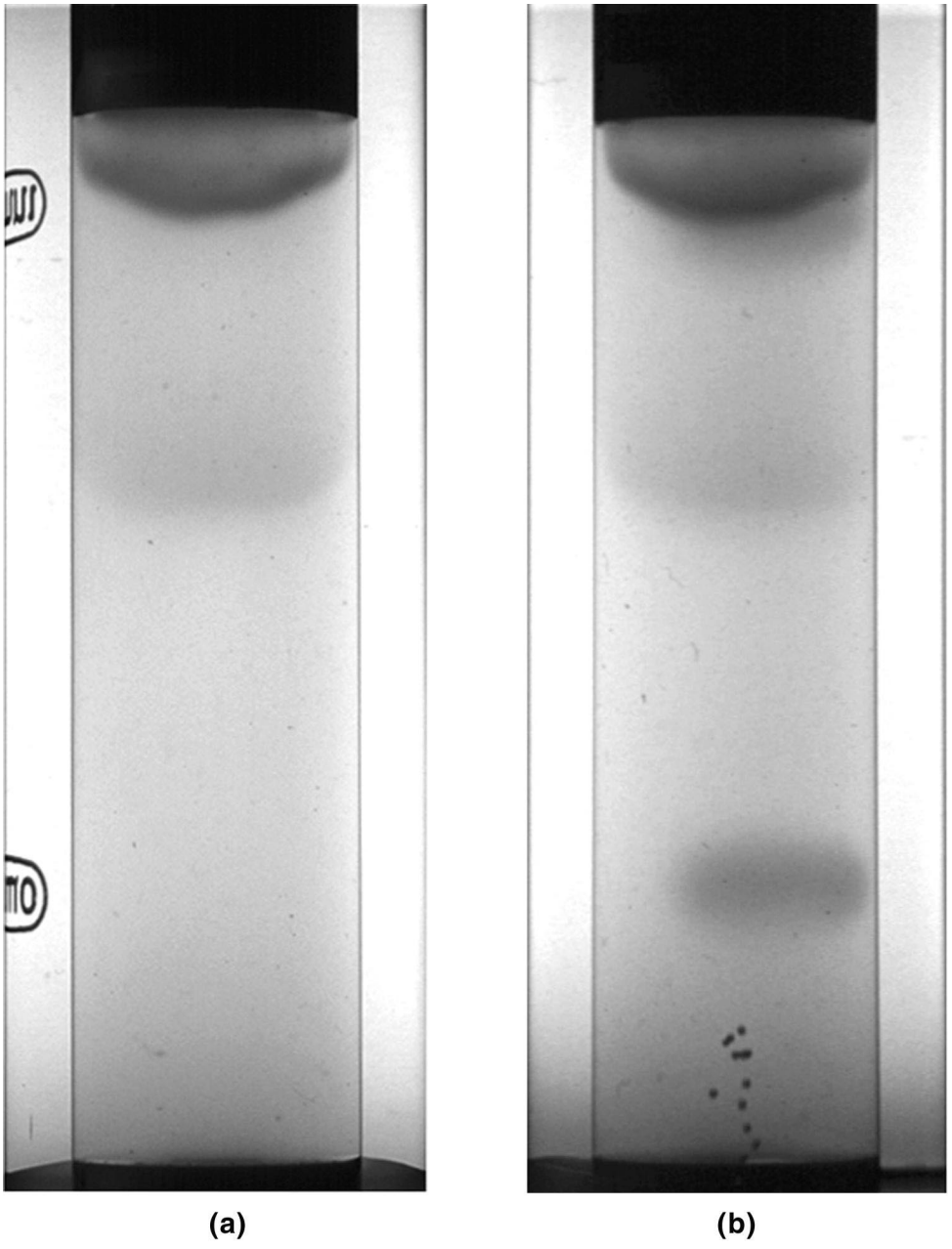

Fig. 18. Photographs of the iodine entering the column that contained the third 10-μm frit and displayed poor chromatographic performance. (a) Camera 1; (b) camera 2. Flow-rate = 1.5 ml/min.

of the local efficiency across the column remained constant from column to column and the significant differences observed between the results obtained with the different frits must originate from transverse fluctuations of the frit permeability. This is the property that controls the radial distribution of the flow velocity of the mobile phase into the column. If the frit permeability is low, there is also a serious

risk of leaks bypassing the frit entirely and leading to an heterogeneous sample distribution affecting negatively column performance. If the frit permeability is closer to that of the bed, the effect is less dramatic. Still, the homogeneity of the frit is of great importance. To this end, the 10-μm frits tended to behave much better, but even so, the variations observed from frit to frit are significant.

4. Conclusion

Multiaspect visualization is a valuable technique for studying sample distribution throughout a column. Considering only a single aspect of the concentration distribution in the column may cause decisions based on misleading information regarding the flow profile of the sample band. For example, what appeared to be a 'crown-shaped' entrance profile [14] (Fig. 2a) was in fact caused by leakage around the frit edge (Fig. 2c). A sample that appeared to enter the column centrally from one aspect (Fig. 10a), was in fact entering off center when viewed from the second aspect (Fig. 10b). Profiles that appeared flat, but dispersed can in fact be shown to be entering the column heterogeneously. Hence, this visualization technique provides the chromatographer with a valuable means of evaluating, among other things, the performance of head fittings.

The 10-μm frits produced better band profiles than the 2-μm frits. This result is in a large part a consequence of the choice of a packing material with an average particle size of 21 μm to pack the columns. Larger particle beds would probably require coarser frits, smaller particles, finer ones. The selection of the frit size cannot be made entirely independently from the selection of the distributor [13]. In all this work, no distributors were used. It is thus remarkable that entrance profiles as flat as those illustrated in Figs. 11 and 12 could be obtained. This illustrates the important role that an appropriately chosen frit may have on the homogenization of the distribution of the sample concentration at the column inlet.

Those chromatographers who still pack their own columns should certainly pay great attention, probably greater attention than they did in the past, to the selection of the proper frit, depending on the characteristics of the column and the packing material. Those of us who buy their columns might profit from including a few questions regarding frit selection, properties, and specifications in the interviews they give to their suppliers. During the course of this study it became clear to us that standard, commercially supplied end fittings were not always as appropriate as a serious analyst would wish. Perhaps, the 'art' associated with packing columns can also be extended to encompass the 'art' of frit selection and manufacture. Admittedly, there are so far no means to sort out and quantify the actual influence of the frits on the column performance. The main result of our work is to demonstrate that this influence is important.

Acknowledgements

This work was supported in part by Grant DE-FG05-88ER13859 of the U.S. Department of Energy and by the cooperative agreement between the University of Tennessee and the Oak Ridge National Laboratory (ORNL). In addition, we thank Kim Thomas (ORNL) and Mark Barnes (Thompson PhotoStudios, Knoxville) for their assistance in this work.

References

[1] E. Bayer, W. Müller, M. Ilg, K. Albert, Angew. Chem., Int. Ed. Engl. 28 (1989) 1029.
[2] E. Bayer, E. Baumeister, U. Tallarek, K. Albert, G. Guiochon, J. Chromatogr. A 704 (1995) 37.
[3] U. Tallarek, E. Baumeister, K. Albert, E. Bayer, G. Guiochon, J. Chromatogr. A 696 (1995) 1.
[4] V.M. Runge (Ed.), Enhanced Magnetic Resonance Imaging, Mosby, St. Louis, MO, 1989, Chapter 5.
[5] S. Aime, M. Botta, G. Ermondi, J. Magn. Reson. 92 (1991) 572.
[6] D.G. Gadian, J.A. Payne, D.J. Bryant, I.R. Yound, D.H. Carr, G.M. Bydder, J. Comput. Assist. Tomogr. 9 (1995) 242.
[7] U. Tallarek, D. van Dusschoten, T. Scheenen, H. Van As, E. Bayer, G. Guiochon, U.D. Neue, AIChE J. 44 (1998) 1962.
[8] F.G. Lode, A. Rosenfeld, Q.S. Yaun, T.W. Root, E.N. Lightfoot, J. Chromatogr. A 796 (1998) 3.
[9] B.S. Broyles, R.A. Shalliker, D.E. Cherrak, G. Guiochon, J. Chromatogr. A 822 (1998) 173.
[10] R.A. Shalliker, B.S. Broyles, G. Guiochon, J. Chromatogr. A 826 (1998) 1.

[11] R.A. Shalliker, B.S. Broyles, G. Guiochon, Am. Lab. 30 (1998) 124.
[12] R.A. Shalliker, B.S. Broyles, G. Guiochon, Anal. Chem. 72 (2000) 323.
[13] R.A. Shalliker, B.B. Broyles, G. Guiochon, J. Chromatogr. A 865 (1999) 83.
[14] T. Farkas, J.Q. Chambers, G. Guiochon, J. Chromatogr. A 679 (1994) 231.